Advances in Applied Mathematics and Mechanics
Adv. Appl. Math. Mech., Vol. **6**, No. 5, pp. 590-603

DOI: 10.4208/aamm.2013.m289
October 2014

Simulation of Vortex Convection in a Compressible Viscous Flow with Dynamic Mesh Adaptation

C. H. Zhou*

Department of Aerodynamics, Nanjing University of Aeronautics and Astronautics, Nanjing 210016, China

Received 14 July 2013; Accepted (in revised version) 28 February 2014

Available online 23 June 2014

Abstract. In this work, vortex convection is simulated using a dynamic mesh adaptation procedure. In each adaptation period, the mesh is refined in the regions where the phenomena evolve and is coarsened in the regions where the phenomena deviate since the last adaptation. A simple indicator of mesh adaptation that accounts for the solution progression is defined. The generation of dynamic adaptive meshes is based on multilevel refinement/coarsening. The efficiency and accuracy of the present procedure are validated by simulating vortex convection in a uniform flow. Two unsteady compressible turbulent flows involving blade-vortex interactions are investigated to demonstrate further the applicability of the procedure. Computed results agree well with the published experimental data or numerical results.

AMS subject classifications: 65M50, 76M99

Key words: Mesh adaptation, vortex-convection, blade-vortex interaction, unsteady flow, time-dependent problem, shock-vortex interaction.

1 Introduction

Theoretically, a Navier-Stokes solver can capture vortex convection correctly. However, in the practical simulation of a flowfield including vortex convection, the predicted vortex structure may be dissipated quickly because of the inherent numerical dissipation and the insufficient mesh resolution in the region of vortex. Vortex convection appears inevitably in a rotor flowfield. This problem limited the full utilization of Navier-Stokes analysis in the rotary wing aerodynamics.

There are several approaches to address this issue in the simulation of vortex convection. Many researches focused on coupling Navier-Stokes solutions with a separate

*Corresponding author.
Email: chzhou@nuaa.edu.cn (C. H. Zhou)

wake model [1–3]. Among them, the prescribed vortex method [1] (also called perturbation method) is frequently used in the aerodynamic design of a helicopter, the essence of which is to split each dependent variable into a prescribed part (vortex disturbance) and a remaining part. The nonlinearity can not be simulated correctly in this approach, so the perturbation method is not suitable to simulate strong blade-vortex or shock-vortex interactions. Using high-order schemes that have less numerical dissipation is also an attempt to simulate blade-vortex interactions [4,5]. But, compared to low-order schemes, the convergence of high-order schemes is poor for a transonic flow with shock waves present [5].

Mesh adaptation can be an effective approach to reduce the numerical dissipation and preserve the intensity of a convected vortex. Till now, a large number of papers about mesh adaptation for the time-independent problems have been published, while the number of papers addressing unsteady flows is relatively small. For unsteady flows, most of the existing methods for dynamic mesh adaptation adjust the mesh per n time-steps (one adaptation period) using the adaptation indicators based on the initial solution in the current period, and the adapted mesh always lags behind the computed unsteady solution. In order to reduce the phase shift in time between the adapted mesh and the computed solution, the mesh was adapted very frequently [6,7]. However, an important source of error due to solution transferring (by interpolation) from the old mesh to the new one is introduced in this case.

Zhou and Ai developed an approach of mesh adaptation for unsteady flows in [8]. In that approach, there exists no lag between mesh and solution and the adaptation frequency can be controlled to reduce the errors due to solution transferring. In this work, we modify the adaptation indicator and the method of adaptive-mesh generation and apply the approach to the simulation of vortex convection in a compressible turbulent flow around an airfoil.

The outline of this article is as follows. In Section 2, the governing equations and the basic numerical schemes are described in brief. In Section 3, the approach for dynamic mesh adaptation is given. In Section 4, results and discussions for numerical experiments are presented. Finally, in Section 5, this work is summarized and concluded.

2 Governing equations and numerical methods

In this work, a compressible turbulent flow is governed by the following two-dimensional Favre-averaged Navier-Stokes equations

$$\frac{\partial \mathbf{w}}{\partial t}+\frac{\partial \mathbf{f}_i}{\partial x_i}+\frac{\sqrt{\kappa}M_\infty}{Re_\infty}\frac{\partial \mathbf{g}_i}{\partial x_i}=0, \tag{2.1}$$

where Re_∞ and M_∞ are the Reynolds number and Mach number of free stream respectively, κ is the ratio of specific heats of a gas, and $\mathbf{w}$, $\mathbf{f}_i$ and $\mathbf{g}_i$ are the vectors of conserva-

tive variables, the inviscid flux and the viscous flux respectively

$$\mathbf{w}=\begin{bmatrix}\rho\\ \rho u_1\\ \rho u_2\\ \rho E\end{bmatrix},\quad \mathbf{f}_i=\begin{bmatrix}\rho u_i\\ \rho u_1u_i+\delta_{i1}p\\ \rho u_2u_i+\delta_{i2}p\\ u_i(\rho E+p)\end{bmatrix},\quad \mathbf{g}_i=\begin{bmatrix}0\\ \tau_{i1}\\ \tau_{i2}\\ u_j\tau_{ij}-q_i\end{bmatrix}. \tag{2.2}$$

In the above expressions, u_i represents the Cartesian component of fluid velocity, ρ the density, E the total energy, p the pressure which can be calculated from the equation of state

$$p=\rho(\kappa-1)\Big(E-\frac{1}{2}u_iu_i\Big), \tag{2.3}$$

τ_{ij} and q_i are the components of the stress tensor and the heat flux vector, respectively

$$\tau_{ij}=(\mu_l+\mu_t)\Big(\frac{\partial u_i}{\partial x_j}+\frac{\partial u_j}{\partial x_i}-\frac{2}{3}\frac{\partial u_\alpha}{\partial x_\alpha}\Big)-\frac{2}{3}\rho k\delta_{ij},\quad q_i=\frac{\kappa}{\kappa-1}\Big(\frac{\mu_l}{\mathrm{Pr}_l}+\frac{\mu_t}{\mathrm{Pr}_t}\Big)\frac{\partial(p/\rho)}{\partial x_i}. \tag{2.4}$$

In (2.4), k is the turbulent kinetic energy, Pr_l the laminar Prandtl number, Pr_t the turbulent Prandtl number, μ_l the molecular viscosity, and μ_t the turbulent eddy viscosity which must be calculated from a turbulence model.

The governing equations are discretized using the Galerkin finite element approach proposed by Mavriplis and Jameson [9]. The procedure begins by storing flow variables at the vertices of triangle, and the flow variables are approximated by piecewise linear functions. Artificial dissipation terms are adopted to ensure the stability, which are constructed as a bend of undivided Laplacian and biharmonic operators in the conserved variables. For unsteady flows, the discrete equations are integrated in time via a dual-time-stepping scheme [10].

For a turbulence closure, the two-equation SST (Shear-Stress Transport) model proposed by Menter [11] is employed. This model combines different elements of the original $k-\omega$ model and the standard $k-\varepsilon$ model, and accounts for the effect of the transport of the principle turbulent stress in boundary-layers with adverse pressure gradient. It is superior to its alternatives. The turbulence equations are solved separately from the Navier-Stokes equations. The diffusive terms are similarly discretized by the finite element approach, while the convective terms are discretized using a first-order upwind scheme to ensure stability and positivity of the conserved variables of turbulence throughout the integration procedure. In [12], such a strategy for discretization of the turbulence equations has been analyzed in detail and validated by many test cases.

3 Dynamic mesh adaptation for unsteady flows

In the simulation of a flow involving vortex convection, the physical solution evolves with time. The solution-adaptive mesh should follow the phenomena progression. Therefore, mesh adaptation must be performed dynamically.

3.1 Procedure of mesh adaptation

In the present work, the scheme of dynamic mesh adaptation for unsteady flows proposed in [8] is employed. In this scheme, mesh adaptation is performed per n time-steps (one adaptation period). Staring from the initial solution at t_0 in each adaptation period, the instantaneous solution at each time-step $t=t_0+\Delta t,t_0+2\Delta t,\cdots,t_0+n\Delta t$ is predicted firstly. Then, an adaptation indicator that takes into account the solution progression is calculated for each triangle, and a new adaptive mesh is generated for this period. After that, the initial solution at t_0 on the previous old mesh is transferred by a linear conservative interpolation [13] onto the new adapted mesh. Finally, the computation is restarted on the new mesh to obtain the time-dependent solution for this time period. For each adaptation period, the mesh is refined in the regions where the solution evolves and is coarsened in the regions where the phenomena deviate since the last adaptation.

In this adaptation procedure, the mesh is adaptive to the solution progression, so there is no phase shift in time between the adapted mesh and the computed solution. Also, there is no need to adapt the mesh frequently and the errors due to solution-transferring can be controlled.

Of course, when transferring the solution on the old mesh to the new adapted mesh, a higher-order interpolation is more accurate than the linear interpolation. However, for long-time simulations, the conservative interpolation seems to be mandatory as it is less sensitive to the increase of the number of interpolations whereas the standard one will dissipate the solution more and more [13]. The previous numerical experiments in [8] have shown that the P^1-conservative interpolation is better than the standard quadratic interpolation in the long-time simulation of unsteady flows.

3.2 Criteria for mesh adaptation

It is necessary to define an indicator of mesh adaptation which can determine automatically the zones of mesh where some refinement or coarsening are required. In the proceeding numerical simulations, the flow fields involve convection of vortex, vortex-shock interaction, vortex-body interaction, and so on. The gradient of density is employed to capture shock waves, and the vorticity is used to capture boundary layers and vortices. For each element K at each time-step j, the magnitude of vorticity and the magnitude of gradient of density are defined respectively as

$$|\nabla\times\mathbf{u}|_K^j=\int_K|\nabla\times\mathbf{u}|d\Omega,\quad |\nabla\rho|_K^j=\int_K|\nabla\rho|d\Omega. \tag{3.1}$$

For the piecewise linear solution, we have

$$|\nabla\times\mathbf{u}|_K^j=\Omega_K\left|\frac{\partial u_1}{\partial x_2}-\frac{\partial u_2}{\partial x_1}\right|,\quad |\nabla\rho|_K^j=\Omega_K\sqrt{\left(\frac{\partial\rho}{\partial x_1}\right)^2+\left(\frac{\partial\rho}{\partial x_2}\right)^2}, \tag{3.2}$$

where Ω_K is the area of element K.

To identify the region the physical phenomena are passing through in an unsteady flow field, the indicator of mesh adaptation for each triangle K in each adaptation period $[(j_0+1)\Delta t,(j_0+n)\Delta t]$ is defined as

$$E_i(K)=\max_{j_0+1\le j\le j_0+n}\left\{|\nabla\times u|_K^j+|\nabla\rho|_K^j\right\}, \tag{3.3}$$

where i is the index of mesh adaptation period.

Two values of $E_{\max}$ and $E_{\min}$ are specified for the ith mesh adaptation period. The element K is refined if $E_i(K)>E_{\max}$ and K is coarsened if $E_i(K)<E_{\min}$.

As it will be shown in Section 4, the indicator of mesh adaptation based on the direct sum of vorticity and density gradient works well at least in the present numerical experiments. The weighted sum can also be used to define an indicator. However, it is difficult to find a general weighted average between vorticity and density gradient. When the simulated flow involves different physical phenomena, the user-specified parameter in combination of different gradients is the inherent drawback of the adaptation indicators based on the gradients of flow variables.

3.3 Refinement and coarsening

In the mesh adaptation for simulation of unsteady flows, the density of discretization points would vary with the evolving solution of flow. A multi-level refinement/coarsening strategy is employed to adjust the mesh dynamically.

The mesh is regularly refined by dividing a triangle into four similar triangles (by connecting the midpoints of the three edges). This creates a tree structure of triangles, in which a leaf is called a triangle son and a root is called a triangle father. To prevent extremely large gradient of mesh density and keep the geometric integrity of the domain as a whole, the original mesh will not be coarsened in the adaptation procedure. So only a refined triangle will possibly be coarsened by deleting its four sons. As illustrated in Fig. 1, in order to eliminate the "hanging point" generated in the regular refinement and coarsening, the triangle with one hanging point is irregularly refined into two triangles by connecting the hanging point to the opposite vortex of the triangle.

The generation of a new adapted mesh begins by removing all triangles generated by irregular refinement in the last mesh adaptation. Then, the regular refinement is performed for the marked triangles from the top level to the bottom level (the original mesh).

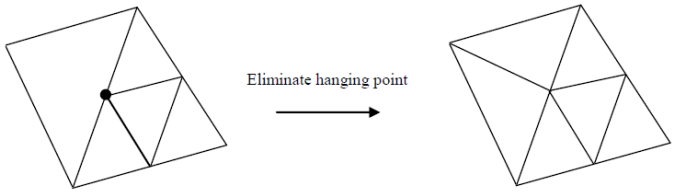

Figure 1: Eliminate the hanging point (•) by irregular refinement.

In the refinement process, any triangle not marked for refinement will be refined if any of its sides has more than one hanging point or it has more than one neighbor that has been regularly refined [14]. The coarsening is performed for the marked triangles from the top level to the second level. In the coarsening process, any triangle marked for coarsening will not be coarsened if it has more than one neighbor that will not be coarsened. If a triangle is not marked for coarsening, the neighbors of its farther triangle will not be coarsened. After the regular refinement and coarsening as described above, each triangle has at most one edge with any hanging point on it and the number of hanging points on the edge is at most one (as shown in Fig. 1). Finally, the triangle with hanging point is irregularly refined into two triangles and a conforming mesh is obtained.

The present approach for generation of an adaptive mesh is quite different from that proposed in [8]. In the previous work, the refinement procedure is based on the longest edge bisection algorithm of Rivara [15], and the coarsening of mesh is carried out by deleting vertices of triangle. Employing the present strategy of multi-level refinement/coarsening, all the triangles on the adapted mesh except those obtained from irregular refinement are similar to the triangles on the original mesh, and any triangle is irregularly refined at most one time. So, after mesh adjusting, the detriment of the geometrical quality of triangles can be controlled. The disadvantage of multi-level refinement/coarsening is the record of some history information, and extra storage is required.

4 Results and discussions

In this section, numerical experiments are performed to show the availability and efficiency of the present dynamic mesh adaptation method in the simulation of vortex convection. Complex blade-vortex and shock-vortex interactions are involved in the simulated flow-fields. These interactions have been investigated widely by numerical simulations [1, 6] and experiments [16–20]. The upper and lower bounds of the adaptation indicator control the extent of refined regions and the density of adapted mesh. As done usually in the conventional mesh adaptation techniques for steady flows, the bounds are determined empirically. On the other hand, to prevent the mesh to be too dense, the minimal size of an adapted mesh $h_{\min}$ is set in advance.

4.1 Vortex model

In this work, the vortex model proposed by Sculley [21] is employed, which is expressed as

$$\frac{v_\theta}{U_\infty} = \frac{\Gamma}{2\pi r}\left(\frac{r^2}{r^2+r_0^2}\right), \tag{4.1}$$

where v_θ represents tangential velocity, r the distance from the vortex center, r_0 the core radius, and Γ the non-dimensional strength of the vortex. Counter-clockwise vortex is

defined as positive. From the constant enthalpy relation, the density field induced by vortex ρ_v can be obtained

$$\rho_v = \frac{2\kappa\rho_\infty p_v}{2\kappa p_\infty - (\kappa-1)\rho_\infty v_\theta^2}. \tag{4.2}$$

In the above formulation, p_v is the induced pressure field which can be determined from the radial momentum equation as follows

$$\frac{dp_v}{dr} = \rho_v \frac{v_\theta^2}{r}. \tag{4.3}$$

The above differential equation is integrated in conjunction with (4.2) from a large value of r where the density and pressure are known, along an inward direction toward the vortex center.

4.2 Vortex convection in uniform flows

In the two test cases of this subsection, the vortex model has a core radius of $r_0 = 0.05$ and a non-dimensional strength of $\Gamma = -0.2$. The vortex convects in an uniform flow at Mach number of $M_\infty = 0.5$. The size of computation domain is 20×2 and the initial mesh has 301×31 nodes. The non-dimensional time-step size is taken to be 1×10^{-3}. Two thresholds for mesh adaptation are set to be $E_{\max} = 2.0\times 10^{-5}$ and $E_{\min} = 5.0\times 10^{-6}$.

At first, the vortex convection in an inviscid flow is considered. In this case, any diffusion of the vortex is due to the numerical discretization. The decay of peak values of the vertical induced velocity is used to measure the numerical dissipation. Fig. 2 shows the decay of the normalized peak-to-peak vertical velocity $\Delta v/\Delta v_0$ with respect to the number of core radii travelled. Three results predicted by the present mesh adaptation approach are presented. In this figure, fine mesh and coarse mesh mean that the minimal mesh size $h_{\min}$ are set to be 2×10^{-3} and 4×10^{-3} respectively, and n represents the number of time-steps in each mesh adaptation period. The averaged numbers of mesh nodes are about 25000 and 22500 for the fine meshes with $n = 200$ and $n = 100$, respectively. The averaged number of mesh nodes is about 14000 for the coarse mesh. We can see that both fine meshes with $n = 100$ and $n = 200$ produced almost the same results and the numerical dissipation of calculations on the finer meshes can be reduced greatly. The results of Tang and Baeder [4] are also plotted in Fig. 2 to make a comparison. The reference results are predicted on a uniform 481×81 mesh by Godunov schemes based on piecewise quadratic reconstruction with slope and curvature computed by sixth order central divided difference (Q6d) or sixth order central compact difference (Q6c). The comparison shows that the present second-order accurate mesh-adapted methodology can produce a better result for the problems involving vortex convection.

The travelling vortex and the adapted mesh in one adaptation period ($n = 100$, $h_{\min} = 4\times 10^{-3}$) are shown in Fig. 3, where the red vorticity contours represent the vortex position at the beginning of the period and the blue contours represent the vortex

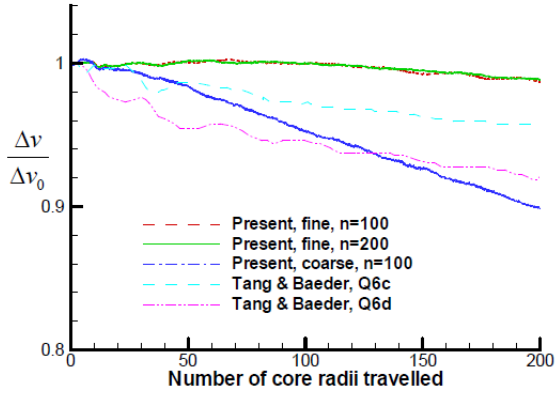

Figure 2: Numerical decay of vortex with respect to convection distance (inviscid flow).

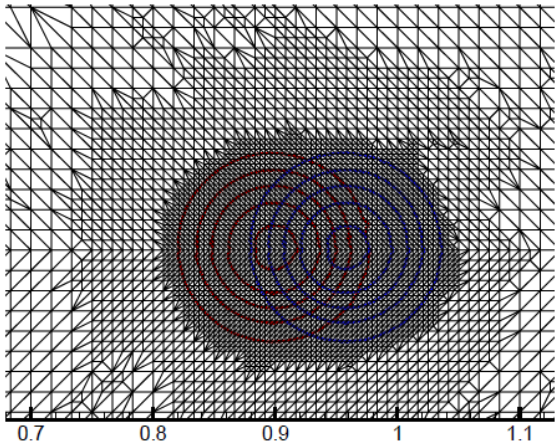

Figure 3: Travelling vortex and adapted mesh in one adaptation period ($n=100$, $h_{\min}=4\times10^{-3}$).

position at the end. With the present mesh adaptation approach, the vortex is always travelling within the region where the mesh is refined.

Secondly, the vortex convection in a laminar flow at Reynolds number of $Re_\infty=3.6\times10^6$ is simulated. At this flow condition, the physical dissipation is very small. Mesh adaptation is performed per $n=100$ time-steps with $h_{\min}=2\times10^{-3}$. The decay of the peak-to-peak vertical velocity is plotted in Fig. 4, together with the result obtained by Oh et al. also on solution-adaptive meshes [6]. The averaged node number of adapted meshes in the present calculation and that in the calculation of Oh et al. are very close to each other. It can be seen obviously that the present mesh adaptation strategy produces a better result. In the procedure of the conventional dynamic mesh adaptation of Oh et al., the mesh is adjusted frequently ($n=10$) and the error due to solution transferring by interpolation may be larger. The conservation of interpolation is also important, but it was not mentioned in [6].

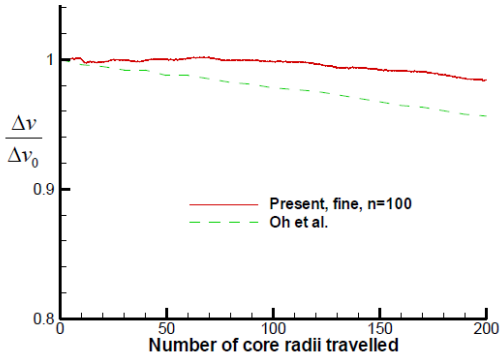

Figure 4: Numerical decay of vortex with respect to convection distance (viscous flow).

4.3 Shock-blade-vortex interaction

The case considered in this subsection is the interaction of vortex with a NACA0012 airfoil in a flow of freestream Mach number $M_\infty=0.8$ and Reynolds number $Re_\infty=3.6\times10^6$. The airfoil is at zero angle of attack. The vortex is initialized far upstream at a distance of 5 chord lengths from the leading edge of the airfoil and at 0.26 chord length beneath the airfoil. The non-dimensional strength of the vortex Γ, based on the freestream velocity and the chord length, is -0.2. The vortex model has a core radius of $r_0=0.05$. To simulate accurately the boundary layers near the body surface, high aspect-ratio triangles are generated around the surface in the original mesh.

The Navier-Stokes equations are first solved to obtain steady solutions, and then the vortex is released at the initial position. In the calculation, the non-dimensional time-step size is taken to be 5×10^{-4}, and the mesh adaptation is performed for every 100 time steps. The minimal mesh size $h_{\min}$ is set to be 4×10^{-3}. Two thresholds for mesh adaptation are set to be $E_{\max}=4.0\times10^{-5}$ and $E_{\min}=1.0\times10^{-5}$.

When the vortex convects downstream beneath the airfoil, the flowfield will evolve and the mesh will be adapted dynamically to follow the evolving of physical phenomena. The progression of adapted meshes and pressure iso-lines at four instantaneous times is shown in Fig. 5. We can see that the intensity of vorticity has been preserved, and the wake and the shocks on the upper and lower surfaces of the airfoil have also been captured well. The shock on the lower surface distorted $(t=5.5)$ and then bifurcated $(t=6.0)$ due to the strong vortex-shock interaction. The bifurcation dissolved away as the vortex convects downstream $(t=6.5)$. The phenomena described above can also be observed in the adaptive-mesh calculation of Oh et al. [6]. In Fig. 6, variations of lift coefficient and moment coefficient (about the quarter chord point) with the instantaneous vortex position are presented. To make a comparison, results of Oh et al. [6] and Srinivasan et al. [1] are also plotted in this figure. The results of the present work are close to those of Oh et al. obtained by a conventional dynamic mesh adaptation, but differ a little from those in [1] where a vortex-prescribed approach was used to alleviate the numerical dissipation but the nonlinearity of vortex-shock interaction could not be simulated well.

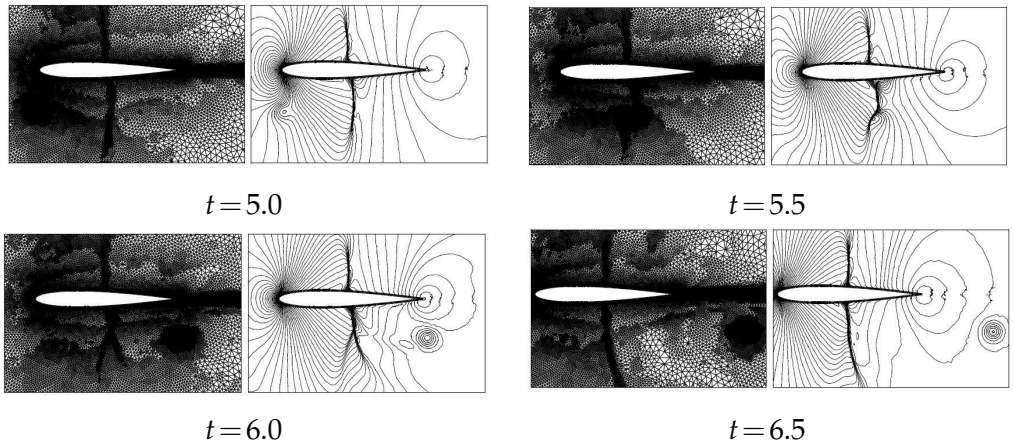

Figure 5: Instantaneous adapted meshes (left) and pressure contours (right).

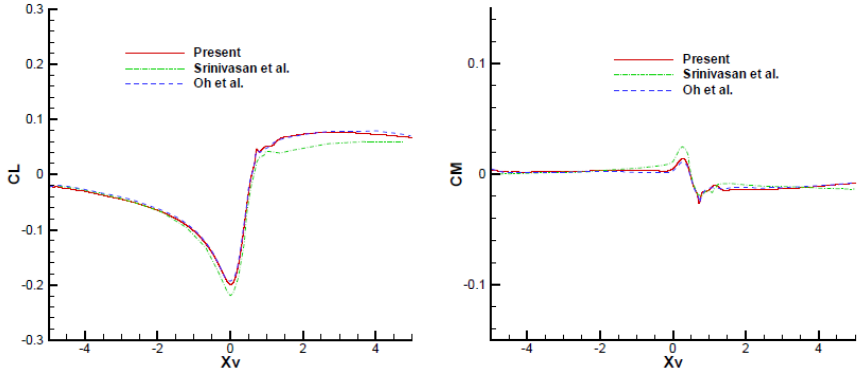

(a) (b)

Figure 6: Variations of lift (a) and moment (b) coefficients with instantaneous vortex position.

4.4 Head-on blade-vortex interaction

In this subsection, simulation of the blade-vortex interaction under the experimental condition of Lee and Bershader [16] is performed. The head-on collision of a vortex and a NACA0012 airfoil was investigated in the experiment. The Mach number of freestream M_∞ is 0.5 and the Reynolds number Re_∞ is 1.29×10^6. The airfoil is also at zero angle of attack. The initial vortex has a core size of $r_0=0.018$ and the non-dimensional strength of $\Gamma=-0.283$. It is released at a distance of 5 chord lengths ahead of the airfoil nose. In this simulation, the non-dimensional time-step size is set to be 2×10^{-4}, and the mesh adaptation is performed for every 300 time steps. The minimal mesh size and the thresholds for mesh adaptation are the same as taken in the subsection 4.3.

Fig. 7 displays the time sequence of adapted meshes, computational density contours and experimental holograms [16] as the vortex approaches and collides with the leading

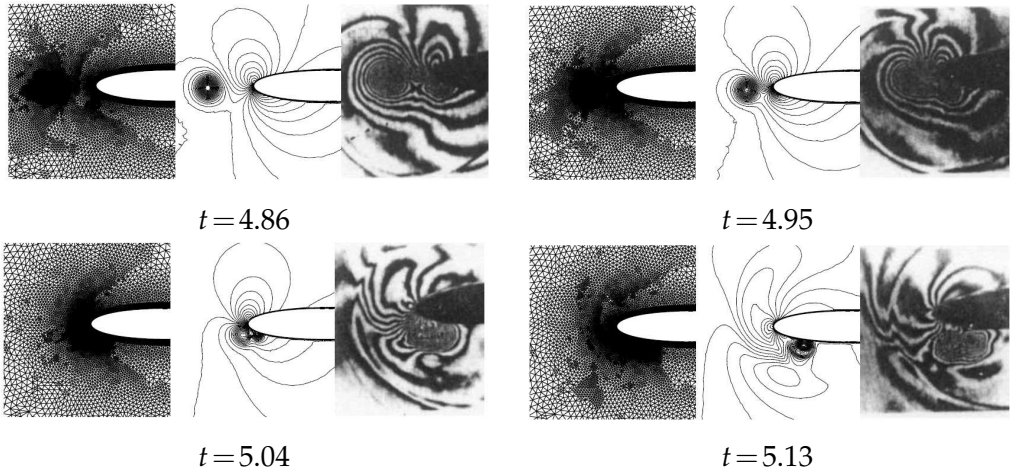

Figure 7: Close-up view of the head-on collision (Left: adapted mesh; Middle: computational density contours; Right: experimental holograms [16]).

edge of the airfoil. The current calculation predicts well the most pertinent features of the flow observed in the experiment, such as oscillation of stagnation point, flow separation and bubble growth on the lower surface. In the experiment of Lee and Bershader, time histories of pressure on the upper and lower surface for three locations near the airfoil nose were measured. In Fig. 8, the results of the current calculation, experiment dada and the Navier-Stokes results of Oh et al. [6] and Lee and Bershader [16] are plotted together to make a quantitative comparison. First of all, the results of the present work are in fair agreement with those of Oh et al. in whose work mesh adaptation was also performed. For the upper surface, the magnitude of pressure peak and the slopes of the pressure traces match the experimental data better than the results of Lee and Bershader due to the utilization of adaptive meshes. The predicted pressure peaks appear to occur slightly earlier than the measured ones. For the lower surface, the pressure peaks and oscillations due to flow separation and bubble moving have been captured. The differences of amplitude are apparent. In the opinion of the author, this is likely due to the different turbulence models used in calculations, or the larger time interval of data collecting in the experiment. The adapted meshes and pressure contours at later time-levels are shown in Fig. 9. The generation and propagation of a compressive wave have been captured as in the work of Oh et al. [6].

5 Summary and conclusions

A mesh adaptation procedure is applied to simulate unsteady flow-fields containing vortex convection. In each adaptation period, the mesh is adjusted dynamically to follow the evolving phenomena. There is no lag between the adapted mesh and the computed solution, and the errors due to solution-transferring from the old mesh to the new one

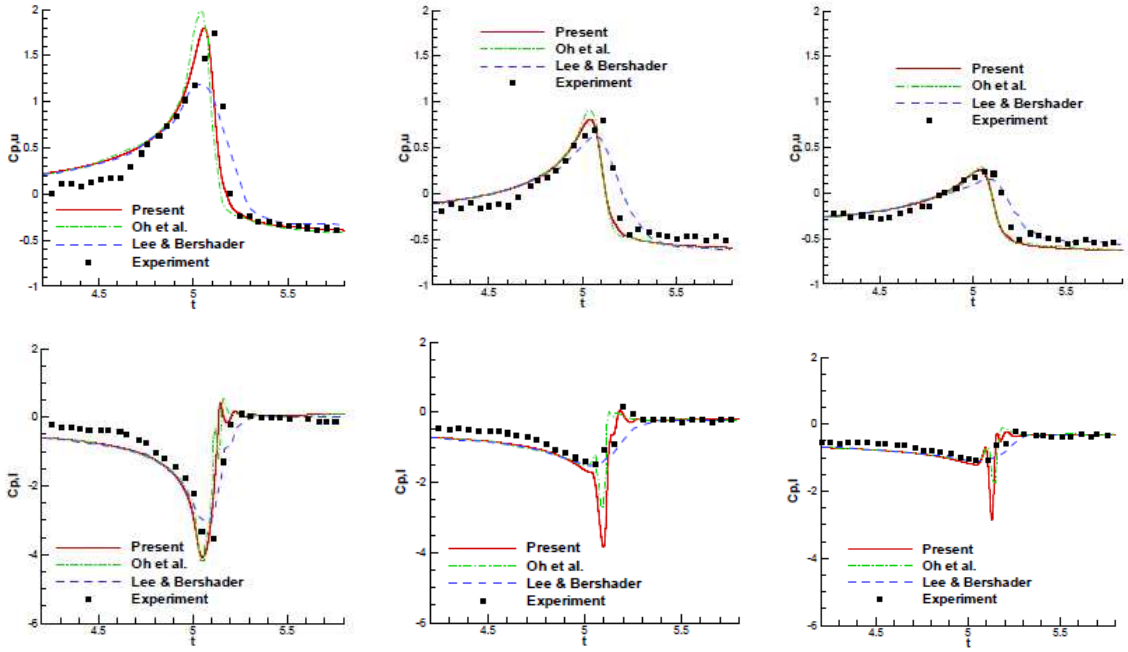

$x/c=0.02$ $x/c=0.05$ $x/c=0.10$

Figure 8: Time history of pressure coefficients at surface locations near leading edge (Top row: upper surface; Bottom row: lower surface).

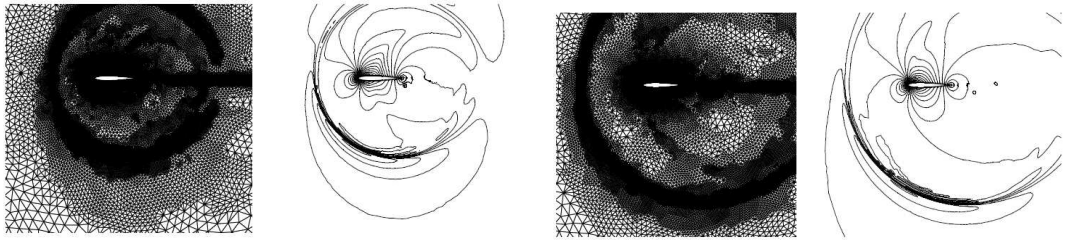

$t=6.00$ $t=6.50$

Figure 9: Instantaneous adapted meshes and pressure contours.

can be reduced by controlling the frequency of mesh adaptation.

By comparing the numerical dissipation in the simulation of vortex convection in a uniform flow with those of the referenced high-order or mesh-adapted simulations, the efficiency and accuracy of the present procedure are validated. The applicability of the procedure is further demonstrated by the numerical experiments on two unsteady flows involving blade-vortex or shock-vortex interactions. Computed results agree well with the experimental data or numerical results available in literature. It is shown that the unsteady flow structure can be captured well and the numerical dissipation can be reduced effectively by using the present dynamic mesh adaptation.

Acknowledgements

This work has been supported by National Science Foundation of China under Grant 11072113.

References

[1] G. R. SRINIVASAN, W. J. MCCROSKEY AND J. D. BEADER, *Aerodynamics of two-dimensional blade-vortex interaction*, AIAA J., 24(10) (1986), pp. 1569–1576.
[2] R. K. AGARWAL AND J. E. DEESE, *Euler calculation for flowfield of a helicopter rotor in hover*, J. Aircraft, 24 (1987), pp. 231–238.
[3] G. R. SRINIVASAN AND W. J. MCCROSKEY, *Navier-Stokes calculations of hovering rotor flowfields*, J. Aircraft, 25 (1988), pp. 865–874.
[4] L. TANG AND J. D. BAEDER, *Improving Godunov-type reconstructions for simulations of vortex dominated flow*, J. Comput. Phys., 213 (2006), pp. 659–675.
[5] B. E. WAKE AND D. CHOI, *Investigation of high-order upwinded differencing for vortex convection*, AIAA Paper, 95-1719, 1995.
[6] W. S. OH, J. S. KIM AND O. J. KWON, *Time-accurate Navier-Stokes simulation of vortex convection using an unstructured dynamic mesh procedure*, Comput. Fluids, 32 (2003), pp. 727–749.
[7] T. J. BAKER, *Adaptive modification of time evolving meshes*, Comput. Methods Appl. Mech. Eng., 194 (2005), pp. 4977–5001.
[8] C. H. ZHOU AND J. Q. AI, *Mesh adaptation for simulation of unsteady flow with moving boundaries*, Int. J. Numer. Meth. Fluids, 72 (2013), pp. 453–477.
[9] D. J. MARIPLIS AND A. JAMESON, *Multigrid solution of the Navier-Stokes equations on triangular meshes*, AIAA J., 28(8) (1990), pp. 1415–1425.
[10] A. JAMESON, *Time dependent calculations using multigrid with applications to unsteady flows past airfoils and wings*, AIAA Paper, 91-1596, 1991.
[11] F. R. MENTER, *Two-equation eddy-viscosity turbulence models for engineering applications*, AIAA J., 32(8) (1994), pp. 1598–1605.
[12] D. J. MARIPLIS AND L. MARTINELLI, *Multigrid solution of compressible turbulent flow on unstructured meshes using a two-equation model*, AIAA Paper, 91-0237, 1991.
[13] F. ALAUZET AND M. MEHRENBERGER, *P^1-conservative solution interpolation on unstructured triangular meshes*, Int. J. Numer. Meth. Eng., 84 (2010), pp. 1552–1588.
[14] B. D. WELFERT, A Posteriori Error Estimates and Adaptive Solution of Fluid Flow Problems, PhD. Thesis of University of California at San Diego, 1990.
[15] M. C. RIVARA, *Mesh refinement processes based on the generalized bisection of simplicities*, SIAM J. Numer. Anal., 21 (1984), pp. 604–613.
[16] S. LEE AND D. BERSHADER, *Head-on parallel blade-vortex interaction*, AIAA J., 32(1) (1994), pp. 16–22.
[17] C. B. LEE AND S. WANG, *Study of the shock motion in a hypersonic shock system/turbulent boundary layer interaction*, Experiments Fluids, 19(3) (1995), pp. 143–149.
[18] C. B. LEE, *New features of CS solutions and the formation of vortices*, Phys. Lett. A, 247(6) (1998), pp. 397–402.
[19] C. B. LEE, Z. X. HONG, Y. S. KACHANOV, V. I. BORODULIN AND V. V. GAPONENKO, *A study in transitional flat plate boundary layers: measurement and visualization*, Experiments Fluids, 28(3) (2000), pp. 243–251.

[20] C. B. LEE AND S. FU, *On the formation of the chain of ring-like vortices in a transitional boundary layer*, Experiments Fluids, 30(3) (2001), pp. 354–357.
[21] M. P. SCULLEY, *Computation of helicopter rotor wake geometry and its influence on rotor harmonic loads*, Massachusetts Inst. of Technology, ASRL TR-178-1, Boston, MA, 1995.